Energy & Buildings 349 (2025) 116526

Contents lists available at ScienceDirect

Energy & Buildings

journal homepage: www.elsevier.com/locate/enb

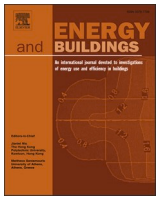

Quantifying the cooling demand of Manhattan using aerial images

Florian Barth [a,*], Kathrin Menberg [a], Matthias Sulzer [b], Philipp Blum [a]

[a] Karlsruhe Institute of Technology (KIT), Institute of Applied Geosciences (AGW), Kaiserstraße 12, Karlsruhe 76131, Germany
[b] Swiss Federal Laboratories for Materials Science and Technology (Empa), Urban Energy Systems Laboratory, Dübendorf, Switzerland

ARTICLE INFO

Keywords:
Aerial images
Instance segmentation
Air-cooled chiller
Cooling tower
Cooling demand
Cooling electricity consumption

ABSTRACT

Cooling demand accounts for a significant share of worldwide electricity consumption, with space cooling being responsible for about 10 % of global electricity consumption, and process cooling making up for 4 % of electricity consumption in the European Union. To implement more efficient district-scale solutions for coupled heating, cooling and thermal storage, spatial information on cooling demand is essential. In this study, a method to quantify installed cooling capacities and cooling demands on building, district and city scale is presented and applied to Manhattan, New York City (NYC). Therefore, heat rejection units of cooling systems are detected in aerial images using deep learning. The cooling capacity of the systems is quantified using a regression model based on visual characteristics of the heat rejection units. The annual operating time is estimated based on building type to calculate the cooling demand. Furthermore, the cooling-related electricity consumption is quantified using energy efficiency ratios and through Monte Carlo simulation to assess the uncertainties of all parameters on different scales. In Manhattan, a total installed cooling capacity of 10.6 ± 0.2 GW, a cooling demand of 10.0 ± 0.2 TWh/a and a cooling-related electricity consumption of 2.82 ± 0.05 TWh/a is quantified. Most of the cooling demand is concentrated in Midtown and the Financial District, with the largest cold consumers being public buildings such as universities and hospitals. Midtown and the Financial District's cooling demands are 171 % and 175 % of the estimated heating demands, respectively. This indicates a high potential for coupled heating and cooling, for example, in the form of seasonal thermal energy storage, especially in and around the named areas in Manhattan.

1. Introduction

Space cooling consumes about 10 % of global electricity and is considered the fastest-growing energy end use in the building sector [1,2]. Additional process cooling consumes about 4 % of electricity in the EU [3,4]. In the future, the demand for space cooling is expected to grow further due to climate change, economic growth, and increasing living standards [1,5]. For process cooling, significant growths are, for example, caused by data centres, which in 2022 consumed 1–1.3 % of global electricity [6] (an estimated 30–40 % by the cooling system [7]), with an annual growth in large data centres of 20–40 % in recent years [6]. To produce cooling energy, currently, almost every cooling system uses a vapour compression cycle [8]. This process is considered relatively energy inefficient, especially when solely air-cooled [1]. More efficient solutions for heating and cooling are required to reduce electricity consumption and possibly related carbon emissions, as well as to relieve the power grid [9]. As heating and cooling demand can synergise, this includes coupling heat and cold production on building, building block or district scale [10,11]. Hereby, seasonal mismatches between heat and cold supply and demand can be compensated using seasonal thermal energy storage systems [12].

In order to assess the potential of areas to benefit from coupled heat and cold production and storage, information on both heating and cooling demand is critical [13]. Thereby, estimations for cooling capacities and demands, or useful cooling energy, can give important indications whether enough waste heat from cold production is available in an area to match the heating demand. However, in particular, information on cooling demand, as well as numbers on installed cooling systems and capacities, are often rare, difficult to obtain and uncertain [2,14]. Also, information on waste heat from process cooling is highly individual and requires additional, site-specific investigation.

On a building scale, cooling demand can, for example, be modelled by approximating physical processes in the building using parameters, such as building size and shape, window-to-wall ratio, thermal transmittance, occupation schedule and climate [15,16]. This gives detailed results on the theoretical cooling demand, required cooling capacities

* Corresponding author.
E-mail address: florian.barth@kit.edu (F. Barth).

https://doi.org/10.1016/j.enbuild.2025.116526
Received 28 May 2025; Received in revised form 2 September 2025; Accepted 26 September 2025
Available online 28 September 2025

and theoretical load curves for planning heating and cooling systems. According to ASHRAE, physical building modelling shall not exceed a mean relative standard deviation of 15 % with monthly calibration data, and 30 % for hourly calibration data [17]. However, simulating buildings is time-consuming and computationally expensive [18]. Therefore, surrogate models are often used to overcome computational and time restraints of physical building models, which replace the physical modelling process with a statistical approach based on modelled input and output data [19]. These surrogate models often predict annual values, but do not provide cooling load curves [19]. Here, the surrogate model by Korolija et al. [20] achieves a relative error between heating and cooling prediction of UK office buildings and ground truth of <10 % for 80 % of the buildings.

To quantify the cooling demand of larger areas, different modelling approaches exist that can be separated into top-down and bottom-up approaches. Top-down approaches use country-scale information and downscale them on districts and cities. Therefore, they often use information such as typical energy consumption by sector, population, gross domestic product, climate, market saturation rate of cooling systems from sales numbers, and sectoral distribution of cold-producing industries to model cooling demand [1,2,21–25]. The smaller the scale at which the cooling demand is modelled, the less precise the information becomes [26]. Thus, many of these approaches only yield information on the theoretical cooling demand on city and country scale, but not on actually utilised cooling on smaller, i.e., building, building block or district scale. While such information can be gathered from sales numbers or market saturation rates, generating spatially resolved information from this top-down information on such small scales is difficult.

Bottom-up approaches, on the other hand, yield small-scale information on mostly theoretical cooling demands and project them onto larger areas with building stock data [23,25]. Information on cooling is often estimated from building properties, occupancy and local climate using physical building models [25], but is occasionally also inferred from monitored buildings [27] or measured district cooling deliveries [23].

Depending on the geographic location, significant discrepancies exist between the theoretical cooling demand of buildings, e.g., for air-conditioning, and the actual cooled floor area [23]. While 90 % of buildings in the US and Japan utilise air-conditioning [1], only 16 % of the theoretical residential and commercial cooling demand of buildings in Europe is covered by cooling systems in reality [28]. These low saturation rates often hinder accurate modelling of the actual cooling energy production through top-down, as well as bottom-up approaches and significantly decrease the spatial resolution of models and significance of their results [22,26]. While the "Pan-European Thermal Atlas", for example, depicts cooling demand on a grid size of 100 m, the authors state that accuracy on scales below 1 km is low [26]. However, high spatial resolution is critical for urban energy planning.

To overcome constraints in spatial resolution and deal with low saturation rates in cooling supply, two studies utilise bottom-up approaches to predict the likelihood of existing cooling systems for individual buildings in Switzerland [29,30]. These studies use building parameters such as floor space, share of occupation and building age, and calibrate their model using information on actual installed cooling systems [29,30]. This data, however, is qualitative, only locally available and the model needs re-calibration for application in other areas. The recently published model "Demand.ninja" combines the strengths of previous cooling demand models [31]. It is based on climate degree days, but incorporates additional site-specific parameters such as building parameters, occupation, solar heat gains, humidity and wind effects, which increase the accuracy of the heating and cooling demand model [31]. Here, the accuracy of Demand.ninja exceeds previous demand models, such as "Hotmaps" by a factor of 1.7 [31]. In modelling the daily heating and cooling electricity demand in the state of New York, Demand.ninja achieves a root mean square error of 1.2 % [31]. However, information on the building's cooling power is necessary to get a quantitative estimation of the cooling demand from "Demand.ninja". This describes the energy required to cool the building by 1 °C and is influenced by the building size, architecture, cooling system efficiency [31] and occupation, reducing the out-of-the-box applicability of the model.

Overall, many cooling demand models focus on specific sectors and uses, such as residential or commercial space cooling, while neglecting commercial and industrial process cooling. However, waste heat from process cooling in particular has a high potential for district heating, cooling and storage systems, with more than half of the produced cooling energy in Europe being process cooling and a constant cooling energy production throughout the year [14]. Also, the market saturation rate of cooling systems strongly impedes statistical quantification of cooling system stock and cooling capacities, for example, from other large-scale cooling demand approaches such as "Heat Roadmap Europe" [28] and is one reason for decreased accuracies of such cooling demand models on building block and district scale [26].

A different approach aims to overcome these sectoral and market saturation constraints and use restrictions of other models by estimating installed cooling capacities with a building-scale resolution [9,32]. Here, the condensers of air-cooled chillers (ACCs) are identified in aerial images, and their cooling capacity is estimated from the number of axial fans. The approach can be extended by training deep learning object detection models to identify ACC condensers and cooling towers (CTs) in aerial images to automatically detect the units and estimate their cooling capacity [32]. This produces spatial information on actually installed cooling systems and their capacities, which is widely unavailable in many countries [14]. This method [32] is also applied in another study to provide data for installed cooling capacities of ACC condensers of hospitals in parts of Germany [33], which otherwise would have required an extensive survey in cooperation with the respective institutions. However, several cooling system types are not considered in previous studies, such as forced draft CTs, which have a market share of up to 40 % amongst CTs [34], and packaged rooftop units (RTUs), which supply 58 % of the commercial floorspace in the US [35]. Furthermore, previously trained object detection models could not detect small ACC condensers with one or two fans, resulting in an underestimation of the actual installed cooling capacity. Finally, the potential of using aerial images and ML algorithms for city-scale energy analysis has so far only been assessed in terms of quantifying cooling capacities [9,32], but not yet for estimating cooling demands, which is essential for urban energy planning [13].

Thus, this study presents an approach to estimate installed cooling system capacities, building cooling demand and cooling-related electricity consumption in Manhattan, NYC, based on the automated detection of various types of cooling systems from aerial images. Firstly, the respective cooling systems, the collection of aerial training images for their detection, and the detection algorithm are elaborated. This is followed by the quantification of cooling capacities, corresponding evaluation procedures and adjustments for further application, and methods to estimate cooling demands and cooling electricity consumption in Manhattan. Subsequently, results are presented to evaluate the detection algorithms and the quantification of cooling capacities. Finally, application results for the entire area of Manhattan are displayed and compared, and possible synergies of heat and cold production and thermal storage are discussed. Additionally, the implications and limitations of the employed approach are pointed out.

2. Methods

The method presented comprises the following steps (Fig. 1):

a) data collection for the different heat rejection units for training and testing the object detection models (Section 2.1),

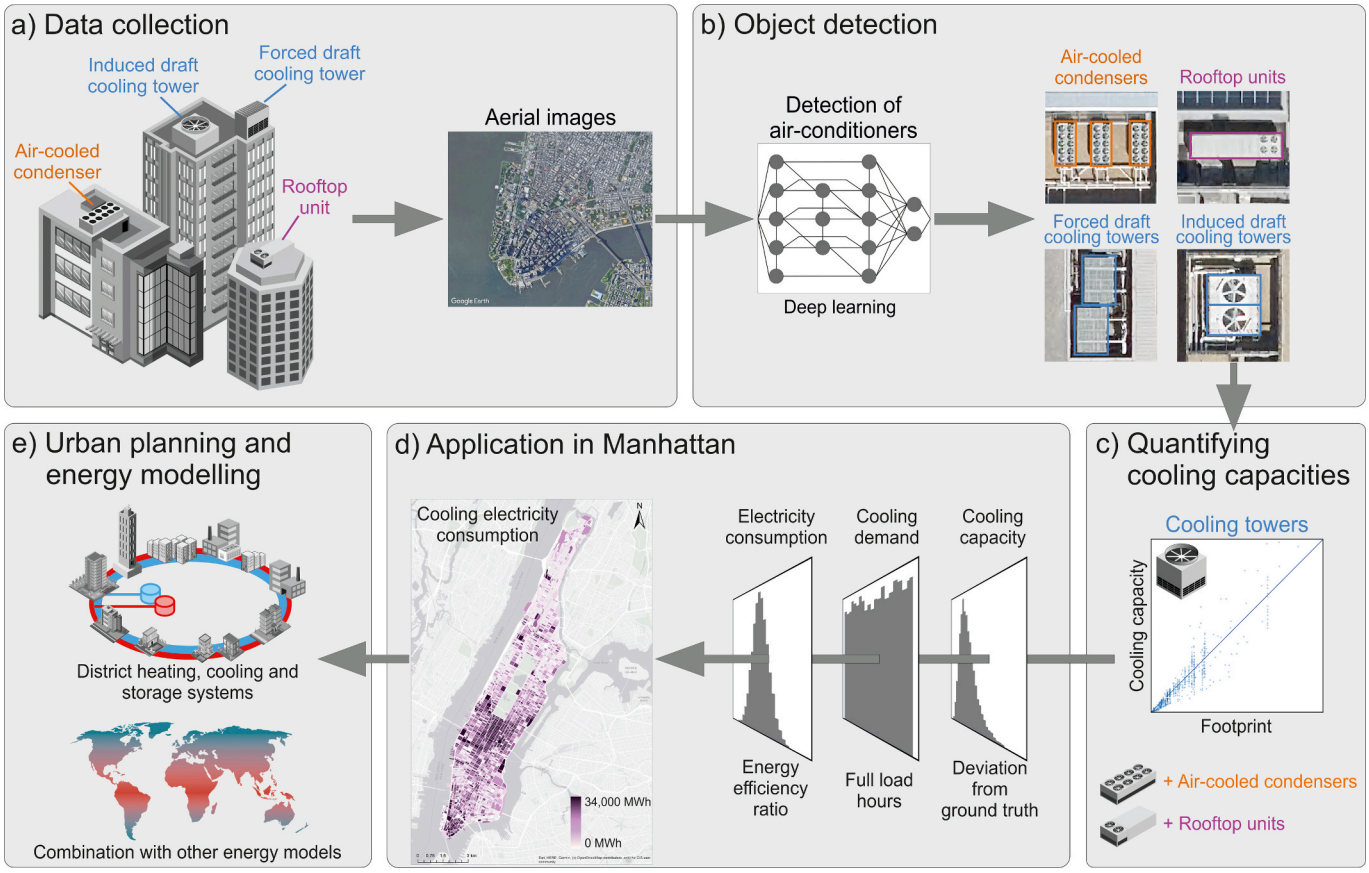

Fig. 1. Workflow for the developed method. (a) Data collection: Aerial images for different heat rejection units are collected; (b) object detection: Units are detected using deep learning; (c) quantifying cooling capacities: The nominal cooling capacity of detected units is estimated via regression models; (d) Application to Manhattan, NYC: The cooling capacity, annual cooling demand and electricity consumption are estimated. (e) Urban planning and energy modelling: The generated information can be used for urban energy planning and to enhance other energy models.

b) object detection via the instance segmentation algorithm Mask R-CNN [36] (Section 2.2),
c) quantifying cooling capacities using regression models, and adjustment to real-world data (Section 2.3),
d) estimating cooling capacities, building cooling demand and cooling-related electricity consumption in Manhattan using Monte Carlo (MC) simulation (Section 2.4).

2.1. Data collection

There are different types of (vapour compression) cooling machines, and their usage within entire cooling systems varies widely across different building types and different regions of the world [37]:

1) ACCs and central split ACs. These units operate after the same principle and are mainly distinguished by size. They make use of a vapour compression cycle with spatially separated evaporator and condenser units, and the condenser coils are cooled by ambient air [38]. Typically, the condenser is installed outside the building (e.g. on the rooftop), while the evaporator is installed within the building. ACC condensers usually utilise characteristic axial fans to cool the condenser coils [32]. These fans are visible in aerial images, enabling identification of the ACC condenser [9,32] (Fig. 1b). Certain central split ACs that utilise condensers with axial fans on rooftops are also included in the ACC category in this study due to their optical and mechanical similarities. The training data contains ACC condensers with a variable number of fans ranging from one to 32.
2) Packaged rooftop units (RTUs). Frequently used for small commercial buildings [35], these single units follow the same principle as ACCs, but contain the evaporator, condenser and compressor in one packaged unit [39]. They are installed on the roof of buildings and directly produce warm or cold air, which is transported directly into the building through ventilation shafts [39]. Not all RTUs possess the option for cooling, but if so, the RTU houses an air-cooled condenser with characteristic axial fans, which are visible from aerial images (Fig. 1b). For the training data, only RTUs with visible condenser fans are included.
3) Water-cooled chillers (WCCs) with a cooling tower (CT). These also utilise a vapour compression cycle. However, the chiller's condenser is cooled by water instead of ambient air. Thus, most WCCs utilise a secondary cooling water cycle with a CT to produce cold water for the condenser from evaporation and conduction [38]. The CTs are typically installed outside the building, and can be categorised into two main unit types. Induced draft CTs utilise a fan on top which sucks air through the CT, while forced draft CTs push air from the bottom through the CT with a fan on the bottom or side [40]. Thus, induced draft CTs are easily identifiable from aerial images by their large axial fan [32] (Fig. 1b). Forced draft CTs are less apparent due to the hidden fan, but can often be identified from their characteristic metal grid on top in combination with additional piping or lateral fan housing (Fig. 1b). Air-cooled condensers, which are sometimes referred to as CT in literature, are differentiated from this category and individually considered in the ACC condenser category.

The considered cooling system categories cover at least 50 % of commercial cold and 43 % of total cold produced in the EU in the form of

ACCs and WCCs [21]; and about 83 % of the commercial cold in the US with ACCs, WCCs and RTUs [35]. More data regarding cooling system type usage would be required to disclose the coverage amongst all cooling sectors more accurately.

A database with aerial images is created to train and test the instance segmentation algorithms for detecting the respective heat rejection units. The database contains 112,800 images with over 300,000 labelled objects (Table 1). These are cropped from aerial images from Berlin (Germany) [41], Cambridge (U.S.) [42], Chicago (U.S.) [43], Frankfurt (Germany) [41], Hamburg (Germany) [41], Los Angeles (U.S.) [41,44], Munich (Germany) [41], New York City (U.S.) [41,45], San Diego (U.S.) [46] and Washington D.C. (U.S.) [47]. A second dataset with 13,781 images and 97,981 labelled ACC axial fans is created to train the second model for detecting the condenser axial fans of ACCs and RTUs. For both models, 90 % of the images are used to train the instance segmentation models, while the remaining 10 % are used to simultaneously evaluate the detection performance to prevent model overfitting to the training data. All images have three bands (RGB). To train single instance segmentation models that are capable of working with various aerial image resolutions, training images are collected at resolutions of 7–30 cm/px and a tile size of 224 px. All training images are used simultaneously in the training process. To augment the training data, tiles are cropped using a sliding window with a stride of 128 px, and six images of each labelled object are cropped by rotating the frame by 60°.

2.2. Object detection of cooling systems

For this study, the instance segmentation algorithm Mask R-CNN [36] is retrained to detect the different heat rejection units and axial fans. Mask R-CNN is a two-stage algorithm with a region proposal network and a subsequent class, box and mask prediction network, which creates a binary mask for the detected objects [36]. Thus, it can precisely outline objects on a pixel scale [36] and measure the footprint accurately. As the backbone of the deep learning model, resnet50 is used to extract the visual features of the heat rejection units of the cooling systems [48]. All models are trained on an Nvidia A5000 graphics processing unit with a batch size of 64 and a learning rate for training of 5.2×10^{-6} to 5.2×10^{-5}.

The detection performance is evaluated by the average precision for the test dataset, which is the integral of the precision-recall curve [49]. Precision and recall are calculated for every possible detection confidence using the following equations:

$$Precision = \frac{TP}{TP + FP} \tag{1}$$

$$Recall = \frac{TP}{TP + FN} \tag{2}$$

with *TP* being the number of true detections, *FP* being false positives and *FN* being false negatives [50].

2.3. Quantifying cooling capacities

Vapour compression chillers remove heat from a room by evaporating a refrigerant at low pressure and release the heat by condensing it under higher pressure in the condenser [38]. For ACCs and central split systems, the condenser is cooled directly by ambient air, so that the rejected heat is proportional to the air flow through the condenser, following the thermal balance equation for air-cooled condensers [51]:

$$\dot{M}_{air} \times c_{air} \times (T_{air_{out}} - T_{air_{in}}) = \dot{M}_s \times r \times x_s \tag{3}$$

where M_{air} is the air flow rate, M_s the steam flow rate, c_{air} the average specific heat, r the condensation latent heat and x_s the steam quality at the inlet. Thus, the nominal cooling capacity is empirically proportional to the number of axial fans of the condenser [9,32]. Similar to previous studies, a regression model is used here to quantify the nominal cooling capacity [9,32], and the number of condenser fans is used as a proxy for the installed nominal cooling capacity of the chiller. The regression for ACC condensers is performed with data from 527 ACC models and their condensers. For RTUs, which follow the same principle as ACCs, but contain the condenser, evaporator and compressor in one housing, the unit's footprint is used in addition to the number of condenser fans in the regression model to quantify the nominal cooling capacity. Accordingly, data on 145 RTU models is used.

WCCs use cold water to cool the condenser, which is typically produced by a CT [38]. Inside the CT, water is sprayed onto a porous fill, while a fan creates an air flow that causes evaporation and heat conduction and thus removes heat from the water [52]. Thus, the CT is sized accordingly to the capacity of the WCC. The nominal cooling capacity of the CT is strongly dependent on the volume of the CT fill and the air flow [52]. The heat transfer rate dQ_w of a CT for a specific CT fill volume can be written as follows [52]:

$$dQ_w = \left(\alpha^*(T_w - T_a) + \frac{\alpha^*}{c_p}(\zeta_s - \zeta_a)\Delta h_{ev}(T_w)\right) dV \tag{4}$$

with α^* being the volumetric heat transfer coefficient, T_w and T_a being water and air temperature, c_p the specific heat at constant pressure, ζ_s the saturation humidity, ζ_a the air humidity, Δh_{ev} the latent heat of evaporation and V the fill volume. The larger the CT, the larger the possible fill volume and absolute air flow through the CT. Thus, in this study, the footprint of the CT is used as a proxy for cooling capacity in the regression model. Two separate regression models for induced and forced draft CTs are set up using data from 634 induced and 325 forced draft CTs. A more detailed overview of the regression analyses is presented in the appendix Table A.1.

The accuracy of the regression models is evaluated using known nominal cooling capacities of ACCs at Campus North of the Karlsruhe Institute of Technology (KIT), which is a research institution in Germany, and CTs in the Financial District and Midtown of Manhattan, NYC (Fig. 2). Values for nominal capacities in Germany are obtained from a survey [9]. Here, 36 ACCs with nominal capacities between 90 and 1200 kW and a total nominal cooling capacity of 14,900 kW are installed. Values for nominal cooling capacities in Manhattan are taken from the New York State cooling tower registry system [53]. Here, 596 CTs with installed nominal cooling capacities between 66 and 39,000 kW and a total nominal cooling capacity of 2.3 GW are installed and used to evaluate the regression models for CTs.

The accuracy of the regression models is evaluated using the relative average deviation (RAD):

$$RAD = \frac{\sum_{i=1}^{n} |y_i - x_i|}{\sum_{i=1}^{n} x_i} \tag{5}$$

with x being the actual installed nominal cooling capacity and y being the estimated nominal cooling capacity. Deviations between the estimated and actual nominal cooling capacity are used in the following to adjust the regression models for the application in Manhattan, NYC.

Table 1
Number of labelled objects within the training and test images for the instance segmentation models.

Unit type		N° of labelled objects
Air-cooled condensers (ACC)		208,906
Rooftop units (RTU)		29,250
Cooling towers (CT)	Induced draft	56,230
	Forced draft	13,840
Axial fans		97,981

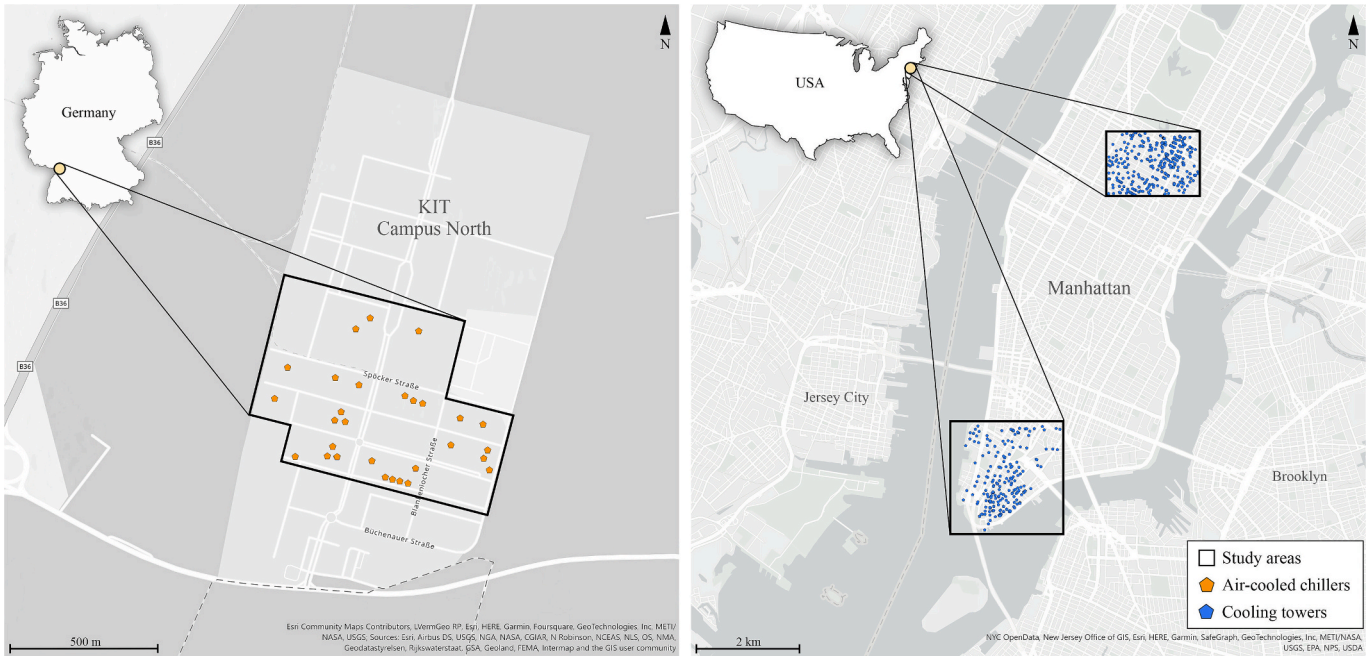

Fig. 2. Areas with installed cooling systems used for the evaluation of the regression models for air-cooled chillers (ACCs) at Campus North of the Karlsruhe Institute of Technology (KIT) in Germany and cooling towers (CTs) in Manhattan, New York City (U.S.).

2.4. *Quantifying the cooling demand of Manhattan*

Heat rejection units of cooling systems in Manhattan are detected using the trained instance segmentation algorithms and aerial images from Google Earth [41] with a resolution of 9 cm/px and orthoimagery mission NYDSOP-6_24_15 [45] with a resolution of 15 cm/px. If necessary, detections are broadly revised and manually corrected to minimise potential discrepancies due to false detections. Then, using the known installed nominal cooling capacities from Germany and Manhattan, the regressions are adjusted to increase the accuracy of the predicted cooling capacities. Therefore, several cooling capacity intervals are defined in which the mean deviation between estimated and actually installed nominal cooling capacities in the interval is used to adjust the estimated capacity (Fig. 3). Additionally, for each interval, the standard deviation of the estimated cooling capacity is calculated. Therefore, a probability density function (Pearson III) is derived from the mean, standard deviation and skewness of the deviations between estimated and actual cooling capacities at KIT and in Manhattan [54]. In

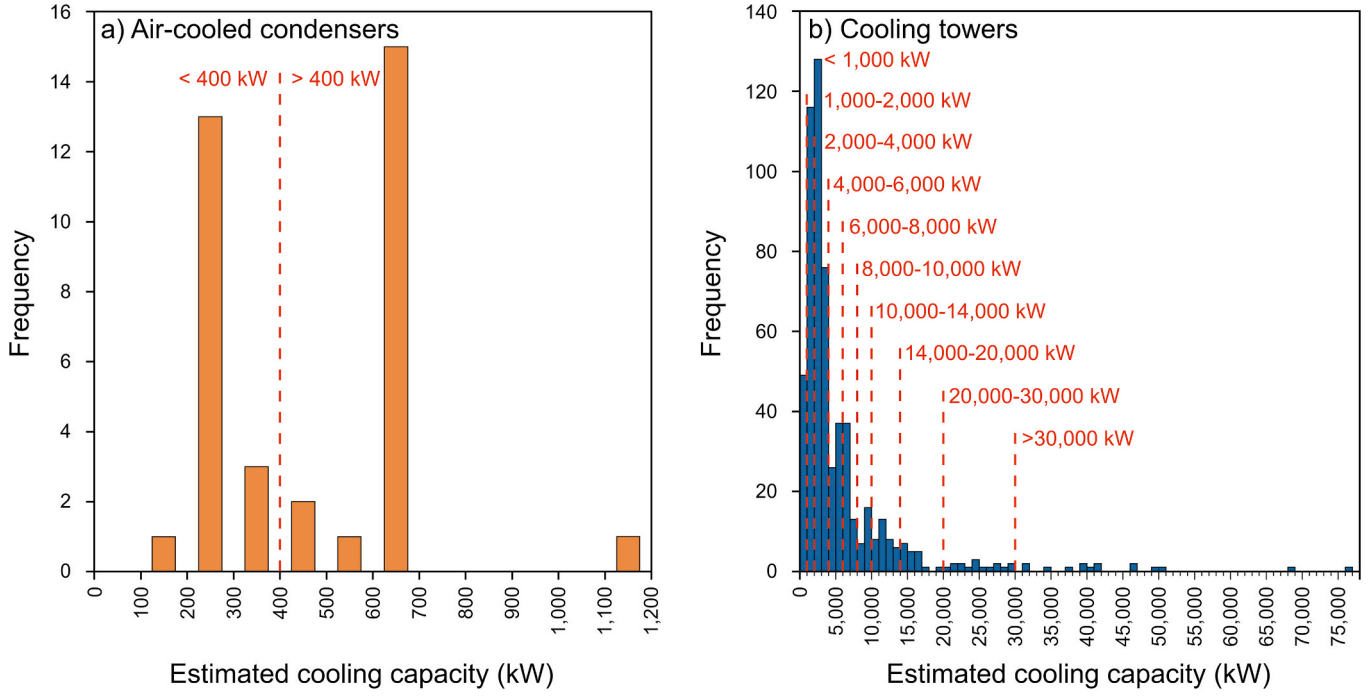

Fig. 3. Histograms for the number of condensers of air-cooled chillers (ACCs) at the Campus North of the KIT (a) and cooling towers (CTs) in Manhattan, NYC (b) for their respective estimated nominal cooling capacity. Red lines mark the intervals for adjusting the regression models and the Monte Carlo (MC) simulation. (For interpretation of the references to colour in this figure legend, the reader is referred to the web version of this article.)

the MC simulation for the application in Manhattan, 500 random deviation values are generated based on this distribution for each detected cooling system to generate 500 cooling capacity values, from which the mean and standard deviation are then calculated. For ACC condensers and packaged rooftop units, two intervals (<400 kW and >400 kW) with approximately equal numbers of units are considered (Fig. 3a). For CTs, the larger dataset and broader range of cooling capacities allows ten capacity intervals to be created for the MC simulation (Fig. 3b). However, the number of units per interval decreases with increasing cooling capacity, with only 15 units having an estimated cooling capacity >30,000 kW.

From the installed cooling capacity of a chiller, the annual useful cooling energy can be calculated using the following equation [55,56]:

$$E_{th} = Q_{th} \times EFLHc \tag{6}$$

with E_{th} being the useful cooling energy, Q_{th} being the nominal cooling capacity and *EFLHc* being equivalent full load cooling hours. EFLHc describe the theoretical operating time of a cooling system at full load to produce the same useful cooling energy as achieved under varying part load operation in the respective buildings in reality [55,56] and are directly related to the building occupancy defined by the different building types [57]. For the sake of simplicity, we here refer to the useful cooling energy as cooling demand. EFLHc values are available for various building types for a particular climate, whereas the cooling capacity is normalised in the modelling of these EFLHc values [57]. For this study, EFLHc values for NYC and New Jersey are used to estimate the operating time of cooling systems in Manhattan [57–59] (Table 2). From the ranges displayed in Table 2, uniform distributions are defined for each building type, based on which 500 random EFLHc values are generated. For application in Manhattan, Equation (6) is solved 250,000 times for each detected cooling system to cover every possible combination of the 500 previously calculated cooling capacity values and 500 EFLHc values. Thus, 250,000 cooling demand values are obtained, from which again the mean and standard deviation for each detected system are derived. In Manhattan, building types are inferred from the Pluto map [60]. For mixed-use buildings, information from the map is used to quantify the share of floor space for the corresponding purpose. The map is also used to remove false detections outside the regular building parcels, such as on streets.

The annual cooling related electricity consumption is linked to the useful cooling energy according to the following equation:

$$E_{el} = \frac{Q_{th} \times \overline{\mathrm{EFLHc}}}{EER} \tag{7}$$

with E_{el} being the annual electricity consumption and *EER* being the annual energy efficiency ratio of the respective cooling system. For reasons of computational efficiency, mean EFLHc values from Table 2 are used here. While the EER of chillers usually refers solely to the compressor, in this case, the annual performance of the chiller systems includes the compressor, evaporator and condenser of ACCs and RTUs, as well as the additional cooling water pumps and CT fan operation for WCCs. Thus, the EER here represents the factor of annual useful cooling energy to annual electricity consumption of the cooling system. EER values for 26 air-cooled and 35 water-cooled systems are collected from various case studies [61–72] (Fig. 4) These include both simulated and measured values of installed cooling systems. Air-cooled systems in the studied literature have a mean EER and standard deviation of 2.7 ± 0.6 kWh/kWh, while water-cooled systems have a mean EER and standard deviation of 3.9 ± 0.6 kWh/kWh. To quantify the standard deviation of the estimated electricity consumption of cooling systems in Manhattan using MC simulation, Pearson III distributions [54] are derived from the mean, standard deviation and skewness of the obtained EER values from literature. For application in Manhattan, 500 random EER values are generated following these distributions for each detected cooling system based on the unit type and used together with the 500 cooling capacity values in equation (7) to calculate 250,000 values for electricity consumption for each detected cooling system. Subsequently, the mean electricity consumption and standard deviation are calculated.

Based on the annual electricity consumption, the equivalent carbon emissions are calculated as follows:

$$M_{CO_2} = E_{el} \times CDI \tag{8}$$

with M_{CO2} being the equivalent carbon emissions and *CDI* the CO_2-intensity of electricity production. In the New York area, a CDI of 266 gCO_2eq/kWh was recorded in 2021 [73]. Finally, peak water consumption is estimated from the nominal cooling capacity of CTs using the following equation:

$$V_h = \frac{Q_{th}}{3.51\,\frac{kW}{ton}} \times 3\frac{gpm}{ton} \times 0.227\frac{\frac{m^3}{h}}{gpm} \times 0.02 \tag{9}$$

with V_w being the hourly water consumption of cooling towers at nominal cooling capacity. Thereby, the make-up water volume, which is renewed every cycle, is equal to 2 % of the CT water flow rate [74]. The annual water consumption of cooling towers is calculated as follows:

$$V_a = V_h \times EFLHc \tag{10}$$

with V_a being the annual water consumption of cooling towers.

To discuss the accuracy of the estimation of cooling capacities, demands and electricity consumptions, the mean relative standard devia-

Table 2
Range of equivalent full load cooling hours (EFLHc) for different building types in New York City and New Jersey [57–59].

Building type	EFLHc
Low-rise residential (< 3 floors)	507–600
High-rise residential (> 3 floors)	793–954
Office	540–1160
Retail	720–1751
Hospital	1217–2440
Hotel	2918–3108
School	260–861
College and university	658–1208
Public facilities	669
Light industrial	544
Other	736

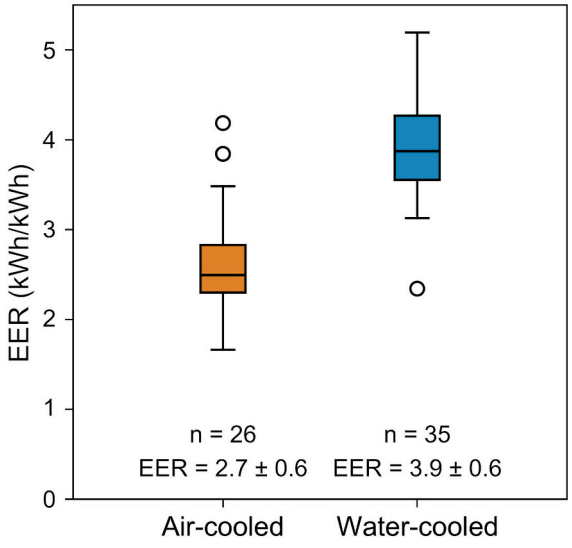

Fig. 4. Annual energy efficiency ratios (EER) of 26 air-cooled and 35 water-cooled cooling systems. Values include designed and measured annual energy consumption of compression, refrigerant and cooling water pumping and condenser and CT fan operation [61–72].

tion is calculated on building, building block, community district and city scale in Manhattan according to the following equation:

$$\overline{RSD} = \frac{1}{n}\sum_{i=1}^{n}\left(\frac{\sigma_i}{Q_{th_i}} \times 100\right) \quad (11)$$

with $\overline{RSD}$ being the mean relative standard deviation, σ being the aggregated standard deviation over a particular scale (building, building block, community district or city scale) and Q_{th} being the sum of the cooling capacity of that same scale. The aggregated standard deviation is calculated using the root of the sum of squares of the individual cooling system standard deviations. For the cooling demand and electricity consumption, Q_{th} is replaced accordingly by the respective parameter.

3. Results and discussion

3.1. Evaluation of the detection algorithms

The instance segmentation model to detect ACC condensers, RTUs units and CTs achieves its best performance after 109 epochs of training (Fig. B.1 a), and both large and small units are reliably detected (Fig. 5). Using the test dataset, the model achieves a mean average precision (mAP) of 0.83 (Table 3). Detection of induced draft CTs works best due to their generally large size and easily recognisable features (Fig. 5c). In contrast, the detection of forced draft CTs performs worse due to the small number of recognisable features (Fig. 5d).

The Mask R-CNN model to detect the axial fans of ACCs is trained for 20 epochs after reaching the best performance (Fig. B.1 b). The instance segmentation models perform well in terms of counting the number of axial fans of ACC condensers and measuring the footprint of CTs with a deviation between the total estimated and actual values of all units of less than 1 % and an R^2 of 0.96 and 0.97 (Table 3).

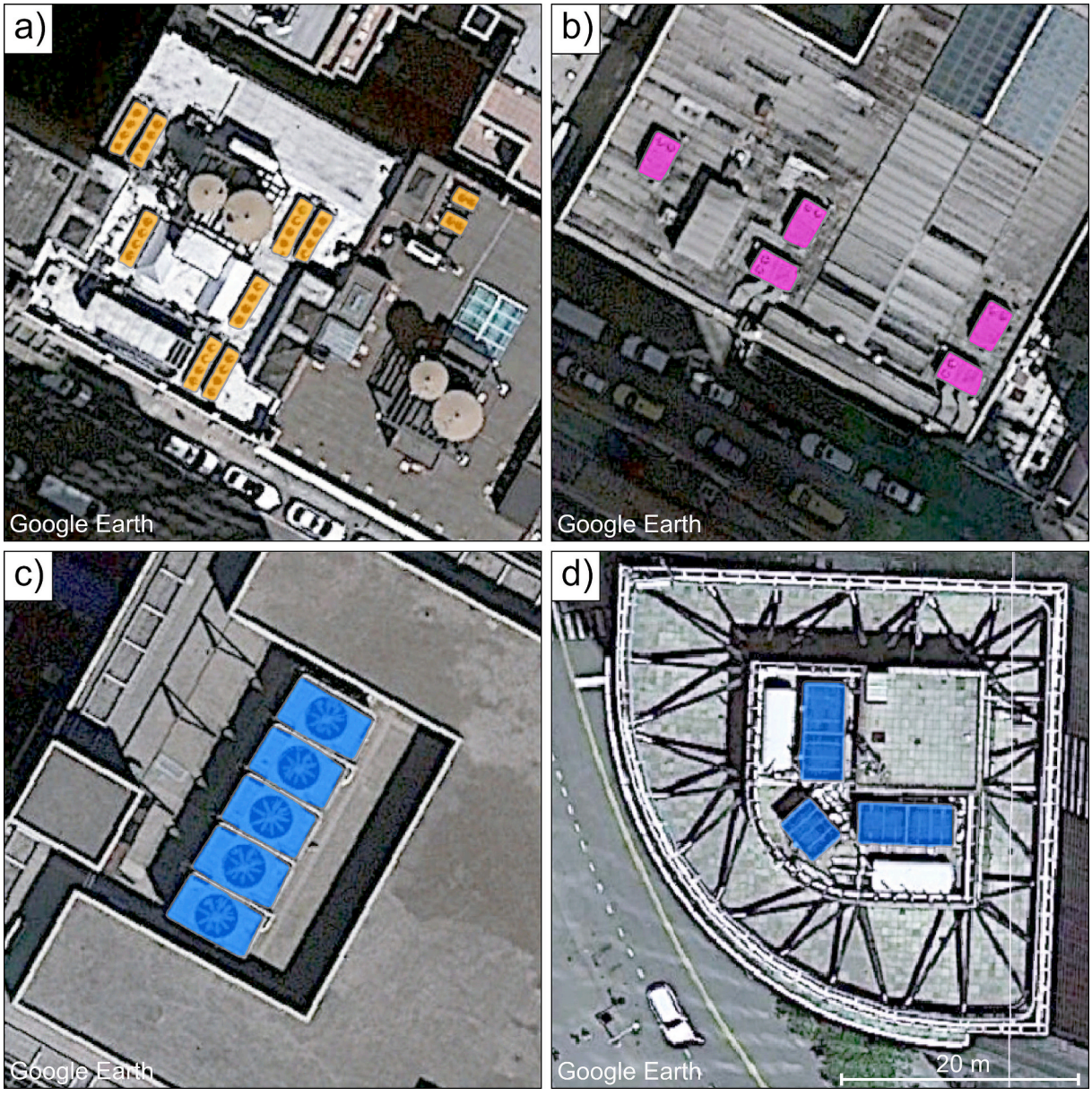

Fig. 5. Sample images for detected air-cooled condensers (ACCs) (a), packaged rooftop units (RTUs) (b), induced draft cooling towers (CTs) (c) and forced draft cooling towers (CTs) (d) in Manhattan.

Table 3
Performance of the object detection models for detecting heat rejection units of cooling systems (detection performance) and estimating their size or number of fans (segmentation performance). To display segmentation performance, the nominal cooling capacity is calculated from the model's predicted unit size or number of fans and compared to the capacity calculated from the actual values.

Unit type		Detection performance	Segmentation performance		
		Average Precision	Total relative deviation	R^2	RMSE (equivalent cooling capacity)
Air-cooled condensers		0.82	−0.6 %	0.96	53 kW
Rooftop units		0.82	+3.8 %	0.84	37 kW
Cooling towers	Induced draft	0.87	−0.3 %	0.97	584 kW
	Forced draft	0.80			

For RTUs, the models are slightly less accurate with a total error of 4 % and an R^2 of 0.84 (Table 3). Larger deviations occur due to the less recognisable fans, leading to miscounting more often for RTUs than ACC condensers. Converted into cooling capacity, CTs show a larger RMSE, while RTUs show the smallest RMSE. However, the RMSE of CTs is the smallest compared to their high cooling capacities. This is because unit size impacts segmentation performance, with the highest relative deviations occurring for the smallest units and those with the fewest fans.

3.2. Evaluating cooling capacities

The regression models for the quantification of cooling capacities are evaluated using data on actually installed nominal cooling capacities of ACC condensers from the KIT and CTs from buildings in Manhattan, NYC. At the Campus North at KIT, the total installed nominal capacity of 14.9 MW is overestimated by 7.7 % (16.0 ± 0.09 MW) with a RAD of 18.5 %. 95 % of the predicted installed capacities are within a range of ±165 kW (Fig. 6a). In general, the estimation of nominal cooling capacity performs better for larger units (Fig. 6). With a maximum deviation of ±25 %, the estimation is more accurate for ACC condensers with cooling capacities >400 kW than for smaller units (Fig. 6c).

In Manhattan, before the adjustment, the total nominal cooling capacity of 596 CTs (2.3 GW) is overestimated by 23 % (2.8 ± 0.004 GW) with a RAD of 48 %. 95 % of the predictions are within a ±8730 kW

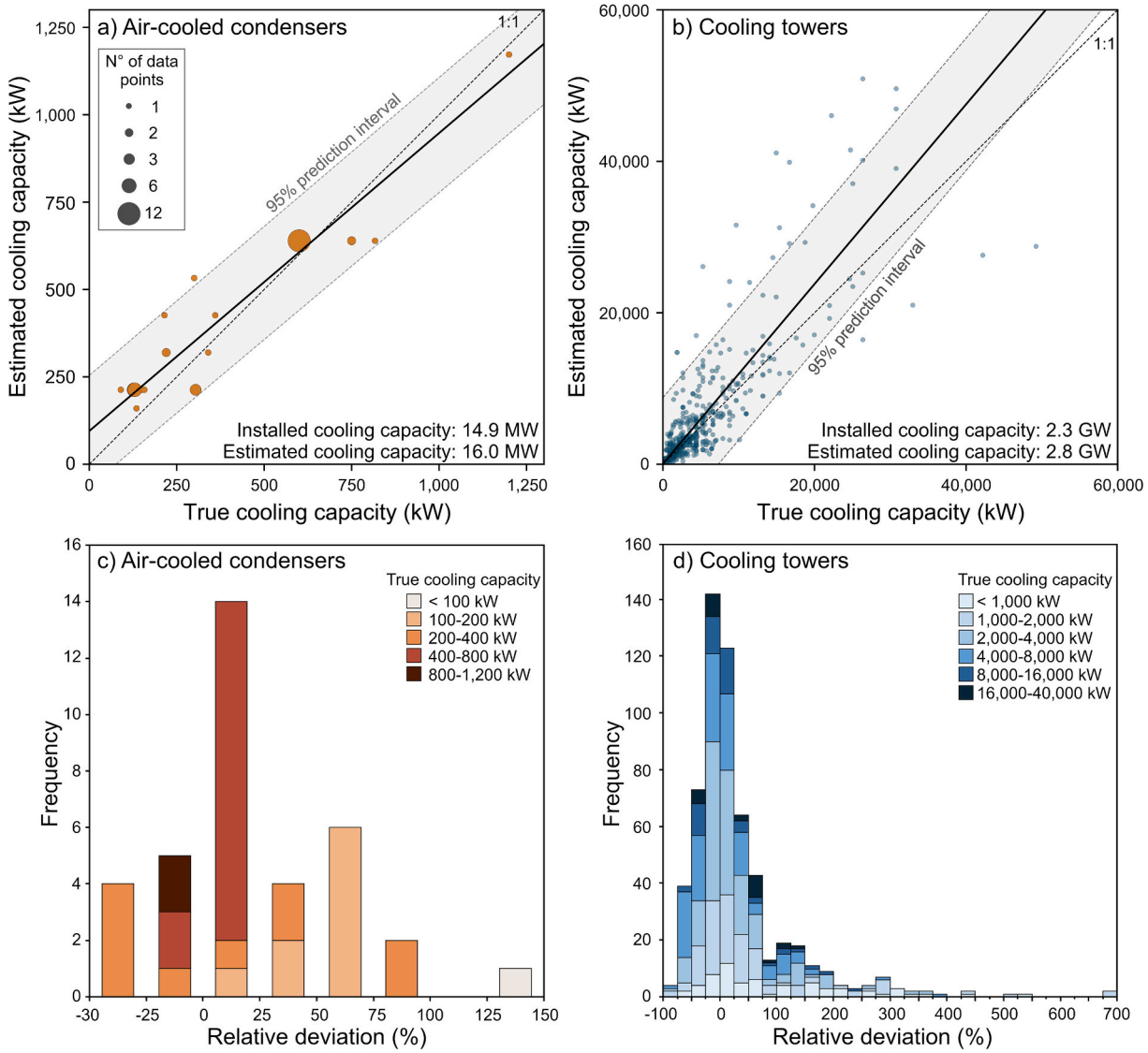

Fig. 6. Estimated and true nominal cooling capacities of air-cooled chillers (ACCs) and their condenser and cooling towers (CTs) before adjustment (a & b). Histograms in c) and d) show the relative deviations between estimations and the actually installed nominal cooling capacity. Colours indicate the true nominal capacities of the machines.

interval (Fig. 6b). CTs with nominal capacities >1,000 kW are estimated more accurately than smaller CTs, while CTs with nominal cooling capacities >16,000 kW are generally over-estimated (Fig. 6b, d). These observed deviations are used to adjust the regression models for the following application in Manhattan. They are also used in an MC simulation to quantify the standard deviation of the cooling capacities. For RTUs, adjustment and distribution for the MC simulation are derived from the ACC condenser values, because both unit types operate after the same principle [39].

3.3. Quantifying the cooling demand of Manhattan

In Manhattan, the instance segmentation algorithm detects about 10,100 ACC condensers, 3600 RTUs and 2500 (multi-cell) CTs. The regression models and the MC simulation reveal a total installed nominal cooling capacity of 10.6 ± 0.2 GW (Fig. 7a). With typical operating times for New York City (Table 2), a cooling demand of 10.0 ± 0.2 TWh/a is estimated for the corresponding buildings (Fig. 7b). Considering the EER for the different unit types, the detected systems would consume 2.82 ± 0.05 TWh/a of electricity (Fig. 7c), which is equal to around 18 % of the modeled residential and commercial electricity consumption of Manhattan [75]. When the EER values are used to estimate the peak power input from the installed cooling capacity in summer, a total power input of 2.98 ± 0.05 GW is calculated, which is equal to the capacity of all four operating nuclear reactors in the state of New York [76]. With equivalent carbon emissions of 266 gCO_2/kWh for 2021, the detected cooling systems in Manhattan produce around 750,000 t of carbon emissions per year, equaling 2.2 % of the carbon emissions from electricity production in New York State in 2021 [73]. If all detected CTs of the respective WCCs operated at full load, they would consume 35,000 m^3 of water per hour due to evaporation and water renewal, corresponding to around 14 Olympic swimming pools (50 m × 25 m × 2 m). With typical annual EFLHc per building type (Table 2), CTs in Manhattan are estimated to consume about 33 × 10^6 m^3 water per year, or 13,000 Olympic swimming pools, which is around 2.4 % of NYC's whole annual drinking water supply [77]. This excludes water use related to electricity production in power plants.

The accuracy in Manhattan increases substantially with scale. On building scale, the $\overline{RSD}$ is 51 % for nominal cooling capacity, 53 % for cooling demand, and 55 % for annual electricity consumption. On building block scale (Fig. 7), $\overline{RSD}$ is 33 % for cooling capacity, 34 % for cooling demand, and 34 % for electricity consumption. Aggregated over the scale of the twelve community districts of Manhattan, the $\overline{RSD}$ ranges from 4 % to 5 % and for the entire Manhattan from 1.6 % to 2 %.

While most detected units are air-cooled, ACC condensers only account for 13 % of installed nominal capacity and packaged RTUs for 4 %. 84 % of the installed nominal capacity is related to water-cooled systems with CTs. In this respect, Manhattan differs from the U.S. average, where the majority of cooling energy in commercial buildings is delivered by packaged systems [35]. This is due to the large number of skyscrapers and other large building complexes, such as universities and hospitals, which utilise mainly water-cooled chillers with CTs and are among the largest producers of cooling energy in the city (Fig. 8).

This high amount of cooling of institutions like universities and hospitals results from a combination of large installed cooling capacities and long operating times throughout the year for both air-conditioning and process cooling. Also, large office buildings in the Financial District and Midtown are found to be large producers of cooling energy (Fig. 8g, h).

Applying values from a building stock model of NYC to the buildings in Manhattan, a cooling-related electricity consumption of 2.6 TWh/a in Manhattan is estimated [75], which is 6 % below our estimation. Likewise, carbon emissions would be 6 % below our estimation [75] when the same equivalent carbon emission factor used above is applied [73]. New York City is estimated to consume 7.3 TWh of electricity for space cooling per year, which is about 17 % of total electricity consumption

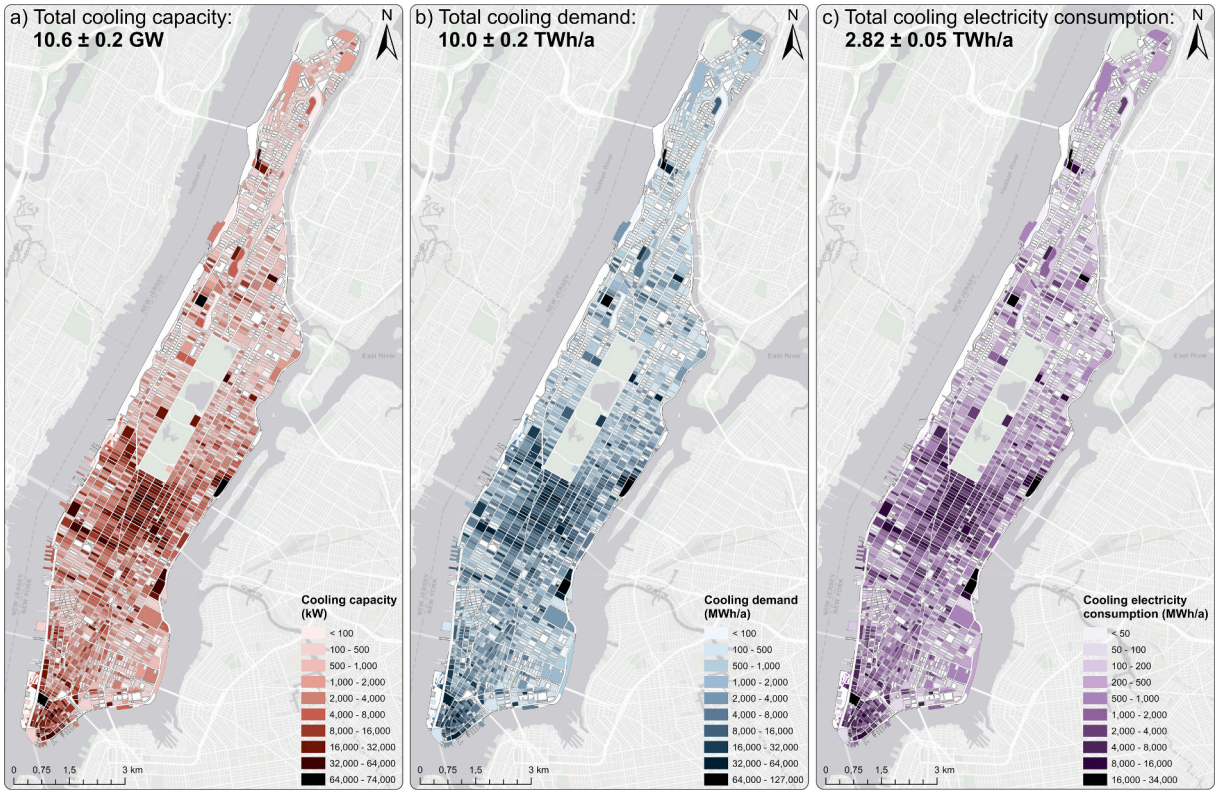

Fig. 7. Estimated nominal cooling capacity (a), annual cooling demand (b) and annual cooling-related electricity consumption (c) in Manhattan. Data is aggregated into building blocks.

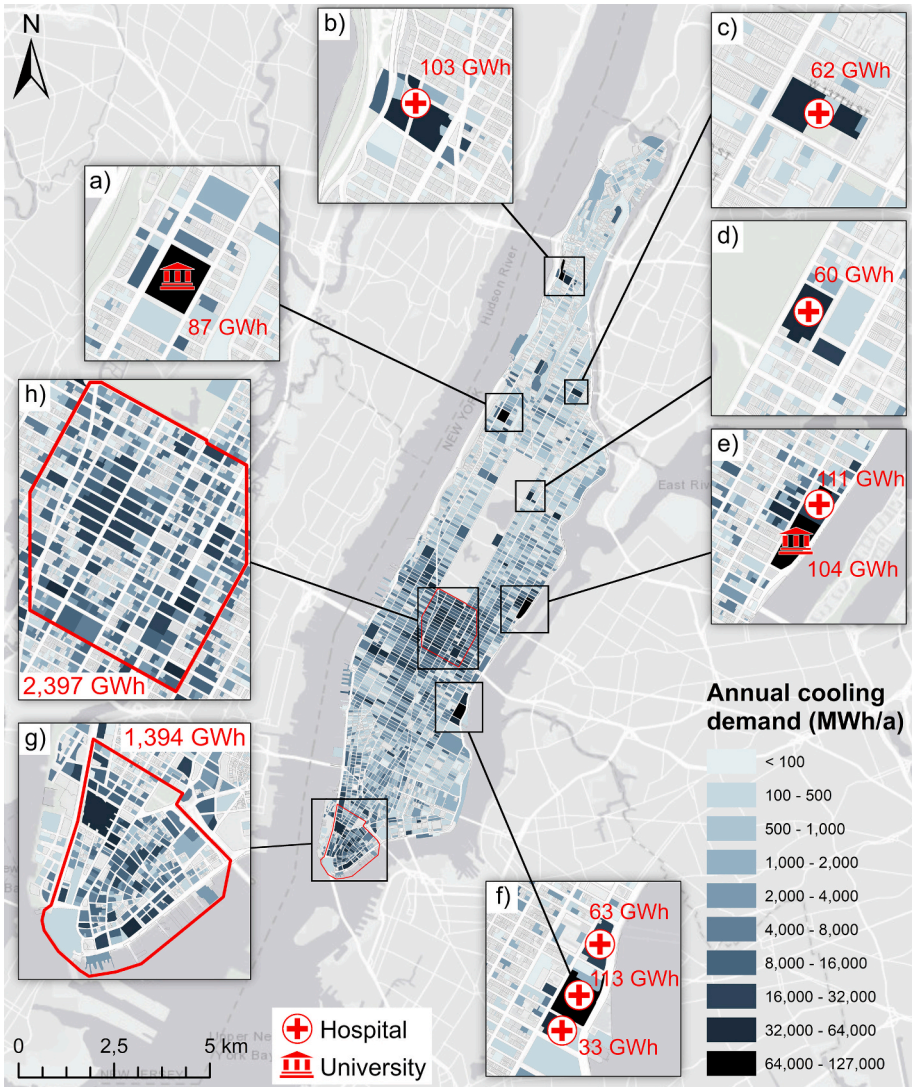

Fig. 8. Estimated annual cooling demand of building blocks in Manhattan. Building (complexes) with particularly high cooling demand are highlighted (a – f) and detailed views of the Financial District (g) and Midtown (h) are shown with building-lot resolution.

[78]. Buildings located in Manhattan are supposed to be responsible for 36 % [75] of the cooling-related electricity consumption of the entire city of New York [78], while in our model, 39 % of NYC's estimated cooling-related electricity consumption [78] is from buildings located in Manhattan. For cooling-related water consumption, comparisons to other studies on city-scale are not comparable, as the share of CTs varies heavily between cities.

Comparing our estimated cooling demand with modelling results for heating demand indicates similar orders of magnitude for Manhattan's heating and cooling demands, as Manhattan's annual space-heating-related fuel consumption is estimated at about 19.7 TWh [75]. With a typical efficiency for gas boilers of 80 % [79], this results in a useful heating energy, or heating demand, of around 15.7 TWh, which equals 157 % of our estimated cooling demand. Locally, however, the cooling demand can even surpass the heating demand. In the Financial District, a heating demand of 0.8 GWh/a is estimated [75], thus, our cooling demand equals 175 % of heating demand (Fig. 8g). In Midtown, a heating demand of around 1.4 GWh/a is estimated [75]. Here, our cooling demand equals 171 % of the estimated heating demand (Fig. 8h). Here, relatively similar heating and cooling demands imply potential for synergies for renewable heat and cold production [80]. Coupled DHC benefits most from simultaneous heating and cooling demands, which may not occur in Manhattan due to the seasonal demand shift and lack of extensive process cooling [31,81]. Seasonal mismatches between heat and cold supply and demand can be compensated using seasonal thermal energy storage systems such as aquifer thermal energy storage (ATES) and borehole thermal energy storage (BTES) systems [10,11]. Hereby, heat and cold are stored in the groundwater or the underground of boreholes and reused for heating and cooling, decreasing electricity consumption and carbon emissions of heating and cooling production by up to 74 % [10,82]. For thermal energy storage systems, relative cost decreases with increasing storage volume, indicating greater potential for buildings with higher heating and cooling demand [83,103]. Manhattan's underground is mainly composed of schist, marble and gneiss with a thin overburden of unconsolidated glacial sediments, which are thickest in the south [84]. As a result, only southern Manhattan is suited for open-loop geothermal systems [85] and ATES systems. Closed-loop systems, on the other hand, are applicable all over Manhattan and standing column wells, which circulate water inside open wells drilled up to 450 m deep into the bedrock, are applicable in most parts of Manhattan [85], enabling the possible use of BTES systems all over Manhattan.

A limiting factor for the application of geothermal systems in the identified areas in Manhattan could be the lack of open spaces for drilling. However, geothermal systems were shown to be able to provide sufficient heat to supply dense urban areas [86]. Especially parks and

other open spaces could be suitable for drilling geothermal boreholes, the largest and most prominent example being the Central Park. If open spaces in the Central Park were utilised, the underground of the park could yield an estimated capacity for heating and cooling (without thermal storage) of up to 1 GW with closed-loop systems and of up to 2 GW with standing column wells [87]. Thermal energy storage could further increase the efficiency of such systems, which can also profit from interacting thermal plumes by closely aligned boreholes [88]. With optimised well positioning and additional seasonal thermal storage in ATES or BTES systems, the potential for geothermal applications would be even higher than the above-reported numbers.

3.4. Implications and limitations

As shown for Manhattan, the presented approach can provide valuable information about actually installed cooling systems of buildings, districts and cities, such as types of cooling, installed nominal cooling capacity, annual cooling demand, power input and annual electricity consumption (Fig. 9). Thereby, the approach sits between physical building modelling and large-scale, data-driven cooling demand modelling. It exceeds physical building models in aspects, such as application speed for districts and cities and can deliver information on actually utilised cooling, such as air-conditioning and process cooling. However, while applicable on building-scale, our approach neither achieves the same accuracy as a detailed physics-based model for an individual building, which according to an ASHRAE standard shall not exceed a $\overline{RSD}$ of 15 % for monthly and 30 % for hourly calibration data [17], nor generates hourly load curves.

Load curves, however, are often required for further planning of heating and cooling systems utilising thermal storage [89]. These thermal storage systems often interact dynamically, utilising short and long-term thermal storage, which are synchronised with the heat source and sink. Thus, overall system efficiency can improve significantly with adequate control strategies [89]. In that respect, coupling our approach with physical prototype building modelling [15] could be a promising possibility for predicting load curves based on typical building occupancy and local climate for the detected cooling systems, thus improving the quantification of cooling demands. Likewise, such physical building models can be enhanced with information on actually utilised cooling systems and cooling capacity, also to, for example, distinguish between theoretical cooling demand and useful cooling energy. On larger scales, this can also increase the significance of surrogate models by offering the possibility to quantify the useful cooling energy alongside the theoretical cooling demand.

Compared to large-scale top-down or bottom-up theoretical cooling demand models, which often focus on city, state or country scale [21], our approach can deliver estimations for actually utilised cooling on building, building block, district and city scale. Hereby, the $\overline{RSD}$ of our estimated cooling electricity consumption in Manhattan (1.7 %) is, although not directly comparable, similar to "Demand.ninja's" normalised root mean square error for daily heating and cooling electricity demand in New York State (1.2 %) [31]. However, our approach is unaffected by the saturation rate of cooling systems, because the utilised systems themselves are identified and quantified as opposed to theoretical (statistical) cooling demands. Thus, it can also identify cooling hot spots, e.g., from process cooling. Application on state or country scales is, however, limited due to application speed and input data requirements, as an extensive image database would be required for such large scales. In this respect, our approach could generate local cooling demand data, which can be upscaled to country scale using a bottom-up approach, e.g., with building data. Until now, insufficient cooling demand input data has been a significant limitation of such bottom-up models [20]; thus, coupling both approaches can be beneficial. Also, combining our approach with other approaches for estimating the theoretical cooling demand (e.g. [23] or [31]) might yield opportunities to spatially assess the saturation rate of cooling systems. The inferred saturation rate can then indicate protruding investments in cooling [29], and therefore help city and energy planners to pre-empt decentralised solutions, e.g., DHC networks, or to target awareness campaigns for thermal storage solutions.

With its relatively high resolution compared to other large-scale models, our approach can help to build cooling cadasters, similar to

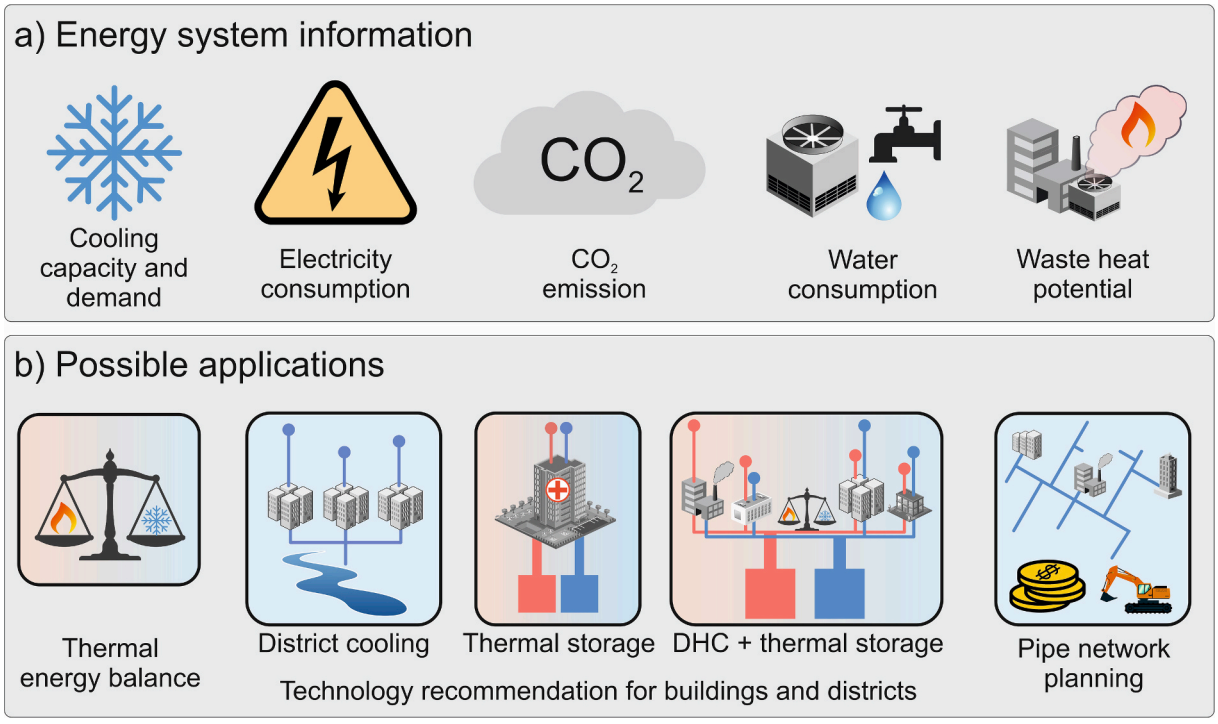

Fig. 9. Obtainable information from the presented approach on the energy sector (a) and possible applications within the scope of renewable urban energy planning (b). DHC = district heating and cooling.

heating cadasters, such as the "Wärmekataster Brandenburg" [90]. Such cadasters can support feasibility studies to plan district solutions [81,91]. They can also help plan efficient shallow geothermal, as well as ATES and BTES systems [92,93].

Another important factor related to cooling is waste heat. The latter is often unused and rejected into the atmosphere using ACCs or WCCs with CTs, neglecting potential heating synergies for nearby buildings. Commercial and industrial process cooling, in particular, is difficult to quantify with conventional cooling demand modelling approaches [81]. While previous studies used, for example, the number of employees of heat-producing industries as a proxy for the amount of waste heat [94], our method can directly estimate the waste heat potential of detected cooling systems. One previously identified large producer of cold in an industrial area in Germany [32], is now integrated into a generation four district heating system [95].

While our method has potential for application within the scope of urban energy planning, it also has certain limitations. If heat rejection units are not clearly identifiable from aerial images, they will not be detected. This applies, for example, to smaller ACs on the side of buildings, as observable on "Google Street View" for many buildings in the residential areas of northern Manhattan [96], as well as units with radial fans instead of axial fans and units covered by roofs or other building structures. Likewise, our approach will yield less relevant results in areas with already existing district cooling systems. While the cooling capacity can be quantified from aerial images for systems with CTs, such as in Hamburg, Germany [97], it is not possible to identify connected buildings without additional information. If the systems utilise, e.g., lake water for cooling, such as in Geneva [98], the systems will remain undetected which will result in an underestimation of cooling capacities and demand in an area. However, city or energy planners applying our approach are likely to be aware of district-scale energy systems. In this sense, the presented method provides minimum values for the number of installed cooling systems and demand within the investigated area.

Uncertainties on building scale due to deviations between estimated and installed nominal cooling capacities are another limitation, especially for CTs (Fig. 6). Additionally, operating conditions, such as ambient and fluid temperatures, fan speeds, internal pressures and refrigerant, influence both the actual cooling capacity at certain times, as well as the efficiency of the cooling systems and thus their annual electricity consumption. Likewise, the age of the cooling system can impact the energy efficiency, as newer systems typically achieve higher efficiencies than older ones [99]. Similarly, modern low-energy buildings and refurbished buildings may require less frequent chiller operation due to better insulation or electrochromic windows, resulting in a potential reduction of EFLHc and thus cooling demand for these buildings in this approach. For the refurbishment of buildings, however, changes in cooling system installation can be monitored over time by comparing aerial images from different years.

Other factors that impact the estimated cooling demand and electricity consumption are free cooling and the existence of backup systems. While the amount of free cooling could be estimated based on building type and climate (e.g. for data centres), uncertainties remain regarding the quantification of electricity consumption. In addition, the object detection algorithm cannot distinguish between active and backup systems, likely overestimating cooling demand and electricity consumption for specific buildings. Usually, data on backup systems is not available and not universally applicable to the buildings in Manhattan or other cities. One branch of buildings, where backup systems are common, are data centres. For example, tier III data centres, which have the largest market share [100], usually employ N + 1 redundancy, meaning that for a cooling system with N chillers, one additional chiller is installed as backup [101]. However, even with such information, it is not possible to characterise the actual share of active to backup systems without further internal knowledge. Similarly, this study does not resolve the utilisation of heat recovery systems, which may increase efficiencies of the installed cooling systems and result in an overall decrease in cooling-related electricity consumption [102]. Finally, for re-use in other studies, site-specific EFLHc are required for the application in other regions, as EFLHc will vary based on, e.g., climatic conditions and usage patterns [57]. Typical values are obtainable from different organisations, such as ASHRAE [57], but could also be modelled from physical building models, such as [15].

4. Conclusion

This study introduces an approach to quantify installed nominal cooling capacities of cooling systems, annual building cooling demands and related annual electricity consumptions in Manhattan based on easily accessible aerial images. Instance segmentation models are trained to detect air-cooled condensers of chillers and central split ACs, packaged rooftop units and induced draft and forced draft cooling towers of water-cooled chillers from aerial images. Their cooling capacity is then estimated from the number of condenser fans and the unit footprint. The cooling demand and annual cooling-related electricity consumption can be estimated using typical operating times and energy efficiency ratios.

Applying the proposed approach to the area of Manhattan in New York City reveals a total cooling capacity of 10.6 $\pm$ 0.2 GW, a cooling demand of 10.0 $\pm$ 0.2 TWh/a and a cooling-related electricity consumption of 2.82 $\pm$ 0.05 TWh/a. The highest cooling demand densities are identified in Midtown and the Financial District, whereas the largest individual consumers in the study area are universities and hospitals. This case study highlights the method's applicability to dense urban and commercial areas.

A significant advantage of the presented approach is its ability to quantify the actual, currently installed space cooling equipment and cooling demand on a building scale, in contrast to commonly estimated theoretical cooling demands. It applies to all building types and usages, including waste heat from commercial and industrial process cooling. The information obtained from our approach allows, for example, to spatially balance obtained cooling demands with existing heating demand data for coupled heating and cooling production with thermal storage.

Declaration of generative AI and AI-assisted technologies in the writing process

During the preparation of this work the author(s) used Grammarly in order to check the spelling and improve the clarity of sentences. After using this tool/service, the author(s) reviewed and edited the content as needed and take(s) full responsibility for the content of the publication.

CRediT authorship contribution statement

Florian Barth: Writing – review & editing, Writing – original draft, Visualization, Validation, Software, Methodology, Investigation, Formal analysis, Data curation, Conceptualization. **Kathrin Menberg:** Writing – review & editing, Supervision, Resources, Methodology, Funding acquisition, Conceptualization. **Matthias Sulzer:** Writing – review & editing, Methodology. **Philipp Blum:** Writing – review & editing, Supervision, Resources, Methodology, Funding acquisition, Conceptualization.

Declaration of competing interest

The authors declare the following financial interests/personal relationships which may be considered as potential competing interests: Florian Barth reports financial support was provided by Federal Ministry for Economic Affairs and Energy (grant number FZK 03EE4040). Kathrin Menberg reports financial support was provided by State of Baden-Wurttemberg Ministry for Science Research and Arts. If there are

other authors, they declare that they have no known competing financial interests or personal relationships that could have appeared to influence the work reported in this paper.

Acknowledgments

The financial support for Florian Barth in the frame of the Geothermal-Based Optimized Energy Systems (GOES) project by the Federal Ministry for Economic Affairs and Energy (BMWE) (grant number FZK 03EE4040), as well as financial support for Kathrin Menberg via the Margarete von Wrangell program of the Ministry of Science, Research and Arts (MWK) (grant number 31-7635.41) of the State of Baden-Württemberg are gratefully acknowledged. A great thank you also to Robin Mutschler (Swiss Federal Laboratories for Materials Science and Technology, Empa), Michael Wetter (Lawrence Berkeley National Laboratory, LBNL), Kenichi Soga (University of California, Berkeley), Ali Hainoun and Daniel Horak (Austrian Institute of Technology, AIT), Alireza Afshari (Aalborg University), Stig Niemi Sørensen (Energy Machines) and the other consortium members of the GOES project for their highly appreciated feedback and expertise regarding heating, cooling and modeling. Additionally, the efforts of data preparation by Efthymia-Eleonora Banakou (Karlsruhe Institute of Technology, KIT) are acknowledged. Thanks also to Nico Peter (Karlsruhe Institute of Technology, KIT) for his expertise in deep learning. Finally, we want to thank the two reviewers for their constructive feedback.

Appendix A. . Regression models

.

Table A.1
Overview of the data for the regression models to quantify the nominal cooling capacity Q_{th} of the heat rejection units of cooling systems.

Unit type		Parameters for regression	Formula	N°of units	Data from manufacturers
Air-cooled condensers		N°of fans n	$Q_{th} = 53.3 \times n$	527	Carrier, Daikin, Emicon, Euroklimat, Evapco, Galetti, Hydrac International, Lennox, TH. Witt Kältemaschinenfabrik, Trane
Rooftop Units		Footprint A in m², N°of fans n	$Q_{th} = 7.0 \times A + 12.2 \times n\text{-}19.4$	145	Carrier, Daikin, Johnson Controls, Lennox, Trane, York
Cooling towers	Induced draft	Footprint A in m²	$Q_{th} = 130.5 \times A$	634	Baltimore Aircoil Company, Bell Cooling Towers, Boldrocchi T.E., CTS Cooling Tower Systems, Evapco, EWK Kühlturm, GEA Energietechnik, Kelvion, Multi Kühlsysteme, Mumme Cooling Tower International, SPX Marley
	Forced draft	Footprint A in m²	$Q_{th} = 132.6 \times A$	325	Baltimore Aircoil Company, Evapco, EWK Kühlturm, SPX Marley

Appendix B. . Training loss curves

.

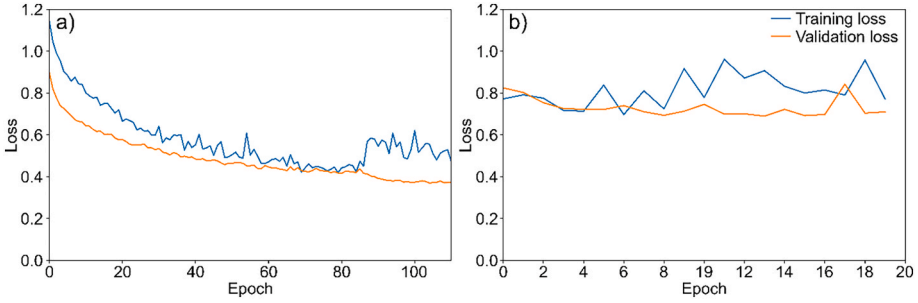

Fig. B.1. Training loss curves of the Mask R-CNN models for the detection of ACCs, CTs and RTUs (a) and ACC axial fans (b) from aerial images. The loss curves are displayed for the training and the test data set.

Data availability

Data will be made available on request.

References

[1] IEA. The Future of Cooling. Opportunities for energy-efficient air conditioning. 2018.
[2] M. Jakubcionis, J. Carlsson, Estimation of European Union residential sector space cooling potential, Energy Policy 101 (2017) 225–235, https://doi.org/10.1016/j.enpol.2016.11.047.
[3] Enerdata. European Union Energy Information 2024. https://www.enerdata.net/estore/energy-market/european-union/ (accessed November 26, 2024).
[4] M. Rehfeldt, T. Fleiter, F. Toro, A bottom-up estimation of the heating and cooling demand in European industry, Energy Effic. 11 (2018) 1057–1082, https://doi.org/10.1007/s12053-017-9571-y.
[5] C.G. Cutillas, J.R. Ramírez, M.L. Miralles, Optimum design and operation of an HVAC cooling tower for energy and water conservation, Energies (basel) 10 (2017), https://doi.org/10.3390/en10030299.
[6] IEA. Data Centres and Data Transmission Networks 2023. https://www.iea.org/energy-system/buildings/data-centres-and-data-transmission-networks#tracking, (accessed April 22, 2025).
[7] EPRI. Powering Intelligence. Analyzing Artificial Intelligence and Data Center Energy Consumption. 2024.
[8] I.A. Ikem, P.A. Ubi, M.I. Ibeh, S.E. Ofem, T.A. Assam, Review of refrigerants for steam compression refrigeration machines, Int. J. Eng. Technol. 10 (2018) 1172–1180, https://doi.org/10.21817/ijet/2018/v10i4/181004056.
[9] S. Schüppler, P. Fleuchaus, R. Zorn, R. Salomon, P. Blum, Quantifying installed cooling capacities using aerial images, PFG – J. Photogrammetry, Remote Sens. Geoinform. Sci. 89 (2021) 49–56, https://doi.org/10.1007/s41064-021-00137-0.

[10] P. Gabrielli, A. Acquilino, S. Siri, S. Bracco, G. Sansavini, M. Mazzotti, Optimization of low-carbon multi-energy systems with seasonal geothermal energy storage: The Anergy Grid of ETH Zurich, Energy Convers. Manage.: X 8 (2020), https://doi.org/10.1016/j.ecmx.2020.100052.
[11] S. Schüppler, P. Fleuchaus, P. Blum, Techno-economic and environmental analysis of an aquifer thermal energy storage (ATES) in Germany, Geotherm. Energy 7 (2019), https://doi.org/10.1186/s40517-019-0127-6.
[12] A. Revesz, P. Jones, C. Dunham, G. Davies, C. Marques, R. Matabuena, et al., Developing novel 5th generation district energy networks, Energy 201 (2020), https://doi.org/10.1016/j.energy.2020.117389.
[13] B. Möller, Mapping the Heating and Cooling Demand in Europe. Work Package 2. Background Report 5 2015.
[14] Fleiter T, Steinbach J, Ragwitz M, Dengler J, Köhler B, Dinkel A, et al. Mapping and analyses of the current and future (2020-2030) heating/cooling fuel deployment (fossil/renewables) Executive summary. 2016.
[15] Department of Energy. Prototype Building Models n.d. https://www.energycodes.gov/prototype-building-models (accessed November 24, 2024).
[16] B. Münch, D. Brandt, Y. Hantouch, A. Karasu, N. Koonenko, A. Küster-Inderfurth et al. Schlussbericht. Eneff: HCBC HochschulCampusBerlin - Charlottenburg. Demonstration eines innovativen Wärmeenergiemanagements für ein Bestandsquartier, 2018.
[17] ASHRAE. Guideline 14-2014. Measurement of Energy, Demand, and Water Savings. 2014.
[18] S. Attia, E. Gratia, A. De Herde, J.L.M. Hensen, Simulation-based decision support tool for early stages of zero-energy building design, Energy Build. 49 (2012) 2–15, https://doi.org/10.1016/j.enbuild.2012.01.028.
[19] P. Westermann, R. Evins, Surrogate modelling for sustainable building design – A review, Energy Build. 198 (2019) 170–186, https://doi.org/10.1016/j.enbuild.2019.05.057.
[20] I. Korolija, Y. Zhang, L. Marjanovic-Halburd, V.I. Hanby, Regression models for predicting UK office building energy consumption from heating and cooling demands, Energy Build. 59 (2013) 214–227, https://doi.org/10.1016/j.enbuild.2012.12.005.
[21] L. Kranzl, M. Hartner, A. Müller, G. Resch, S. Fritz, T.U. Wien, et al. Heating & Cooling outlook until 2050, EU-28. 2018.
[22] L. Frayssinet, L. Merlier, F. Kuznik, J.L. Hubert, M. Milliez, J.J. Roux, Modeling the heating and cooling energy demand of urban buildings at city scale, Renew. Sustain. Energy Rev. 81 (2018) 2318–2327, https://doi.org/10.1016/j.rser.2017.06.040.
[23] U. Persson, S. Werner. Quantifying the Heating and Cooling Demand in Europe Work Package 2 Background Report 4, 2015.
[24] Unternehmen für Ressourcenschutz. Kältemarktanalyse der Stadt Hamburg im Juni 2010, 2010.
[25] L.G. Swan, V.I. Ugursal, Modeling of end-use energy consumption in the residential sector: A review of modeling techniques, Renew. Sustain. Energy Rev. 13 (2009) 1819–1835, https://doi.org/10.1016/j.rser.2008.09.033.
[26] Pan-European Thermal Atlas 5.2 n.d. https://euf.maps.arcgis.com/apps/webappviewer/index.html?id=8d51f3708ea54fb9b732ba0c94409133 (accessed March 6, 2023).
[27] R. Mutschler, M. Rüdisüli, P. Heer, S. Eggimann, Benchmarking cooling and heating energy demands considering climate change, population growth and cooling device uptake, Appl. Energy 288 (2021), https://doi.org/10.1016/j.apenergy.2021.116636.
[28] S. Werner, European space cooling demands, Energy 110 (2016) 148–156, https://doi.org/10.1016/j.energy.2015.11.028.
[29] X. Li, J. Chambers, S. Yilmaz, M.K. Patel, A Monte Carlo building stock model of space cooling demand in the Swiss service sector under climate change, Energy Build. 233 (2021), https://doi.org/10.1016/j.enbuild.2020.110662.
[30] J. Chambers, P. Hollmuller, O. Bouvard, A. Schueler, J.L. Scartezzini, E. Azar, et al., Evaluating the electricity saving potential of electrochromic glazing for cooling and lighting at the scale of the Swiss non-residential national building stock using a Monte Carlo model, Energy 185 (2019) 136–147, https://doi.org/10.1016/j.energy.2019.07.037.
[31] I. Staffell, S. Pfenninger, N. Johnson, A global model of hourly space heating and cooling demand at multiple spatial scales, Nat. Energy (2023), https://doi.org/10.1038/s41560-023-01341-5.
[32] F. Barth, S. Schüppler, K. Menberg, P. Blum, Estimating cooling capacities from aerial images using convolutional neural networks, Appl. Energy 349 (2023), https://doi.org/10.1016/j.apenergy.2023.121561.
[33] M. Noethen, R. Stemmle, N. Siebert, M. Herrmann, K. Menberg, P. Blum, et al., Identifying aquifer thermal energy storage (ATES) key locations for hospitals in Lower Saxony, Germany, Geothermics 130 (2025), https://doi.org/10.1016/j.geothermics.2025.103334.
[34] S. Singh, Global Evaporative Cooling Tower Market Overview. 2025.
[35] Energy Information Administration US. 2018 Commercial Buildings Energy Consumption Survey. 2021.
[36] K. He, G. Gkioxari, P. Dollár, R. Girshick, Mask R-CNN 2017.
[37] J. Adnot, P. Riviere, D. Marchio, M. Holmstrom, J. Naeslund, J. Saba, et al. Energy Efficiency and Certification of Central Air Conditioners (EECCAC), 2003.
[38] B. Kiran Naik, P. Muthukumar. Empirical Correlation Based Models for Estimation of Air Cooled and Water Cooled Condenser's Performance. Energy Procedia, vol. 109, Elsevier Ltd; 2017, p. 293–305. https://doi.org/10.1016/j.egypro.2017.03.070.
[39] T. Pistochini, R. Mcmurry, Emerging Technologies Packaged Roof Top Unit with Integrated Heat Pump and Indirect/Direct Evaporative Cooling Project Manager: Kelly Cunningham Pacific Gas and Electric Company Packaged Roof Top Unit with Integrated Heat Pump and Indirect/Direct Evaporative Cooling ET21PGE1902 Pacific Gas and Electric Company Emerging Technologies Month Year, 2022.
[40] K. Singh, R. Das, An experimental and multi-objective optimization study of a forced draft cooling tower with different fills, Energy Convers. Manag. 111 (2016) 417–430, https://doi.org/10.1016/j.enconman.2015.12.080.
[41] Google. Google Earth Pro 2021.
[42] U.S. Geological Survey. USGS High Resolution Orthoimage, Massachusetts 0.075 meter GSD - 2015; UTM 19N remote-sensing image, 2015.
[43] N. Aldridge, Cook_IL_2012, Cook County, Illinois, 2013.
[44] S. Mills, Los Angeles 2015. 2015.
[45] S. Mills, NYDSOP-6_24_15. 2015.
[46] J. Burroughs, Airbourne Topographic Ortho Report. San Diego, CA 2014 10 cm Ortho, 2015.
[47] DC GIS Group. Aerial Photography (Orthophoto) - 2019. 2020.
[48] K. He, X. Zhang, S. Ren, J. Sun, Deep Residual Learning for Image Recognition 2015.
[49] M. Everingham, J. Winn, The PASCAL Visual Object Classes Challenge 2012 (VOC2012) Development Kit. 2012.
[50] K.M. Ting, Confusion Matrix 2011. https://doi.org/10.1007/978-0-387-301.
[51] S. Bracco, O. Caligaris, A. Trucco, Mathematical models of air-cooled condensers for thermoelectric units, WIT Trans. Ecol. Environ. 121 (2009) 399–410, https://doi.org/10.2495/ESU090351.
[52] N. Milosavljevic, P. Heikkilä, A comprehensive approach to cooling tower design, Appl. Therm. Eng. 21 (2001) 899–915.
[53] Center for Environmental Health. New York State Cooling Tower Registry Weekly Extract 2021.
[54] K. Pearson, Contributions to the mathematical theory of evolution.—II. Skew variation in homogeneous material, Philos. Trans. R. Soc. Lond. A 186 (1895) 343–414, https://doi.org/10.1098/rsta.1895.0010.
[55] D. Korn, W.C. John, Exactly What Is a Full Load Cooling Hour and Does Size Really Matter? 2016.
[56] S. Wang, C. Yan, F. Xiao, Quantitative energy performance assessment methods for existing buildings, Energy Build. 55 (2012) 873–888, https://doi.org/10.1016/j.enbuild.2012.08.037.
[57] S. Carlson, Development of Equivalent Full Load Heating and Cooling Hours for GCHPs Applied in Varous Building Types and Locations. ASHRAE 1120-TRP. 2001.
[58] New York State Joint Utilities. New York Standard Approach for Estimating Energy Savings from Energy Efficiency Programs - Residential, Multi-Family, and Commercial/Industrial Measures. Version 8. 2021.
[59] New Jersey Board of Public Utilities. New Jersey's Clean Energy Program. Protocol to Measure Resource Savings. FY2020. 2019.
[60] Department of City Planning. PLUTO and MapPLUTO 2023. https://nycplanning.github.io/db-pluto/#/ (accessed March 6, 2023).
[61] S. Alonso, A. Morán, M.Á. Prada, P. Reguera, J.J. Fuertes, M. Domínguez, A data-driven approach for enhancing the efficiency in chiller plants: A hospital case study, Energies (basel) 12 (2019), https://doi.org/10.3390/en12050827.
[62] A. Beghi, L. Cecchinato, M. Rampazzo, A multi-phase genetic algorithm for the efficient management of multi-chiller systems, Energy Convers. Manag. 52 (2011) 1650–1661, https://doi.org/10.1016/j.enconman.2010.10.028.
[63] L. Cecchinato, M. Chiarello, M. Corradi, A simplified method to evaluate the seasonal energy performance of water chillers, Int. J. Therm. Sci. 49 (2010) 1776–1786, https://doi.org/10.1016/j.ijthermalsci.2010.04.010.
[64] Y.-C. Chang, C.-R. Su, J.-T. Lu, C.-L. Chen, C.-W. Chen, C.-W. Lee, et al. Application of Air-Cooled Chiller for Comfort and Energy Saving. vol. 2. 2012.
[65] R. Jing, M. Wang, R. Zhang, N. Li, Y. Zhao, A study on energy performance of 30 commercial office buildings in Hong Kong, Energy Build. 144 (2017) 117–128, https://doi.org/10.1016/j.enbuild.2017.03.042.
[66] Y. Chen, C. Yang, X. Pan, D. Yan, Design and operation optimization of multi-chiller plants based on energy performance simulation, Energy Build. 222 (2020), https://doi.org/10.1016/j.enbuild.2020.110100.
[67] F. Oliveira, A. Ukil, Energy Efficiency in Variable Speed Centrifugal Chiller Systems Driven by Synchronous Reluctance Motors. International Conference on Innovative Smart Grid Technologies (ISGT Asia 2018) : 22-25 May 2018, Singapore, 2018.
[68] H.C. Rauser, S. Filippini, Influence of the dry cooler capacity on the efficiency of chillers, REHVA (2013) 34–35.
[69] H. Sha, D. Qi, Investigation of mechanical ventilation for cooling in high-rise buildings, Energy Build. 228 (2020), https://doi.org/10.1016/j.enbuild.2020.110440.
[70] X. Wu, Z. Chen. Performance analysis of a district cooling system based on operation data. Procedia Eng, vol. 205, Elsevier Ltd; 2017, p. 3117–22. https://doi.org/10.1016/j.proeng.2017.10.335.
[71] K. Yang, X. Hao, Y. Lin, Q. Xing, H. Tan, J. Hu, et al., An integrated system of water-cooled VRF and indirect evaporative chiller and its energy saving potential, Appl. Therm. Eng. 194 (2021), https://doi.org/10.1016/j.applthermaleng.2021.117063.
[72] F.W. Yu, K.T. Chan, Chiller system performance benchmark by data envelopment analysis, Int. J. Refrig 35 (2012) 1815–1823, https://doi.org/10.1016/j.ijrefrig.2012.07.003.
[73] Electricitymaps 2023. https://app.electricitymaps.com/zone/US-NY-NYIS (accessed December 5, 2023).
[74] M. Badruzzaman, J.R. Anazi, F.A. Al-Wohaib, A.A. Al-Malki, F. Jutail, Municipal reclaimed water as makeup water for cooling systems: Water efficiency,

biohazards, and reliability, Water Resour. Ind. 28 (2022), https://doi.org/10.1016/j.wri.2022.100188.
[75] B. Howard, L. Parshall, J. Thompson, S. Hammer, J. Dickinson, V. Modi, Spatial distribution of urban building energy consumption by end use, Energy Build. 45 (2012) 141–151, https://doi.org/10.1016/j.enbuild.2011.10.061.
[76] New York Independent System Operator Inc. 2023 Load & Capacity Data Report. Gold Book. 2023.
[77] City of New York. Water Supply n.d. https://www.nyc.gov/site/dep/water/water-supply.page (accessed May 26, 2025).
[78] New York State Energy Research and Development Authority (NYSERDA). Climate Change: Equitable Access to Cooling in New York City. NYSERDA Report Number 21-27. Prepared by Guidehouse, Inc. nyserda.ny.gov/publications. 2021.
[79] M.C. Barma, R. Saidur, S.M.A. Rahman, A. Allouhi, B.A. Akash, S.M. Sait, A review on boilers energy use, energy savings, and emissions reductions, Renew. Sustain. Energy Rev. 79 (2017) 970–983, https://doi.org/10.1016/j.rser.2017.05.187.
[80] F. De Oliveira, S. Schneider, P. Hollmuller, DataRen, a Territorial Energy Demand Modelling Tool. IOP Conf Ser Earth Environ Sci vol. 290 (2019), https://doi.org/10.1088/1755-1315/290/1/012093.
[81] Y. Zhang, P. Johansson, A.S. Kalagasidis, Quantification of overlapping heating and cooling demand for the feasibility assessment of bi-directional systems over Europe, Energy Build. 294 (2023), https://doi.org/10.1016/j.enbuild.2023.113244.
[82] R. Stemmle, P. Blum, S. Schüppler, P. Fleuchaus, M. Limoges, P. Bayer, et al., Environmental impacts of aquifer thermal energy storage (ATES), Renew. Sustain. Energy Rev. 151 (2021), https://doi.org/10.1016/j.rser.2021.111560.
[83] M Herrmann, P Fleuchaus, B Godschalk, M Verbiest, AN Sørensen, P Blum, Capital costs of aquifer thermal energy storage (ATES): a review, Renew. Sustain. Energy Rev. 226 (2026), https://doi.org/10.1016/j.rser.2025.116202.
[84] T. Schmidt, D. Mangold, H. Müller-Steinhagen, Seasonal thermal Energy Storage in Germany, ISES Solar World Congress (2003).
[85] Unites States Geological Survey. Geology of the New York Region Part 1: The Geology of New York State Through Time n.d. https://www.usgs.gov/geology-and-ecology-of-national-parks/geology-new-york-region (accessed June 21, 2024).
[86] Goldman Copeland, PWGC. Geothermal screening webtool. Pre-feasibility. 2018.
[87] C. Tissen, K. Menberg, P. Bayer, P. Blum, Meeting the demand: geothermal heat supply rates for an urban quarter in Germany, Geotherm. Energy 7 (2019), https://doi.org/10.1186/s40517-019-0125-8.
[88] New York City Mayor's Office of Sustainability, USGS. NYC Geothermal Webtool 2018. https://www.nyc.gov/assets/ddc/geothermal/geothermalTool.html (accessed December 4, 2023).
[89] M. Bakr, N. van Oostrom, W. Sommer, Efficiency of and interference among multiple aquifer thermal energy storage systems, A Dutch Case Study. Renew Energy 60 (2013) 53–62, https://doi.org/10.1016/j.renene.2013.04.004.
[90] H. Bastida, C.E. Ugalde-Loo, M. Abeysekera, M. Qadrdan, J. Wu, N. Jenkins. Dynamic modelling and control of thermal energy storage. Energy Procedia, vol. 158, Elsevier Ltd; 2019, p. 2890–2985. https://doi.org/10.1016/j.egypro.2019.01.942.
[91] Con Energy. Erstellung und Weiterentwicklung eines Wärmekatasters für Brandenburg - Projektdokumentation Arbeitspaket 1. 2022.
[92] C. Delmastro, G. Mutani, L. Schranz, The evaluation of buildings energy consumption and the optimization of district heating networks: A GIS-based model, Int. J. Energy Environ. Eng. 7 (2016) 343–351, https://doi.org/10.1007/s40095-015-0161-5.
[93] C. Tissen, K. Menberg, S.A. Benz, P. Bayer, C. Steiner, G. Götzl, et al., Identifying key locations for shallow geothermal use in Vienna, Renew. Energy 167 (2021) 1–19, https://doi.org/10.1016/j.renene.2020.11.024.
[94] R. Stemmle, H. Lee, P. Blum, K. Menberg, City-scale heating and cooling with aquifer thermal energy storage (ATES), Geotherm. Energy 12 (2024), https://doi.org/10.1186/s40517-023-00279-x.
[95] W. Loibl, R. Stollnberger, D. Österreicher, Residential heat supply by waste-heat re-use: sources, supply potential and demand coverage-a case study, Sustainability (switzerland) 9 (2017), https://doi.org/10.3390/su9020250.
[96] Badenova. Wärmeverbund Freiburg-West n.d. https://www.badenovawaermeplus.de/waermeversorgung/waermeverbund-freiburg-west/?accordion_625666=0 (accessed December 13, 2023).
[97] Google. Maps Street View 2024.
[98] City Nord. Fernkältewerk n.d. https://city-nord.eu/de/city-nord/haeuser/fernkaeltewerk (accessed August 15, 2025).
[99] Haszno L. Water from Lake Geneva used to heat and cool buildings 2021. https://houseofswitzerland.org/swissstories/environment/water-lake-geneva-used-heat-and-cool-buildings (accessed August 15, 2025).
[100] T. Hua, M. Yitai, L. Minxia, L. Chuntao, Z. Li, The status and development trend of the water chiller energy efficiency standard in China, Energy Policy 38 (2010) 7497–7503, https://doi.org/10.1016/j.enpol.2010.06.020.
[101] Fortune Business Insider. Data Center Market Size, Share & Industry Analysis, By Component (Hardware, DCIM (Data Center Infrastructure Management) Software, and Services), By Data Center Type (Colocation, Hyperscale, Edge, and Others), By Tier Level (Tier 1 and Tier 2, Tier 3, and Tier 4), By Data Center Size (Small, Medium, and Large), By Industry (BFSI, IT & Telecom, Healthcare, Government, Manufacturing, Retail & E-commerce, and Others), and Regional Forecast, 2025-2032 2025. https://www.fortunebusinessinsights.com/data-center-market-109851 (accessed August 18, 2025).
[102] Pitt W, Iv T, Seader JH, Brill KG. Tier Classifications Define Site Infrastructure Performance. n.d.
[103] M. Rasouli, C.J. Simonson, R.W. Besant, Applicability and optimum control strategy of energy recovery ventilators in different climatic conditions, Energy Build. 42 (2010) 1376–1385, https://doi.org/10.1016/j.enbuild.2010.03.006.